ISSN 1063-780X, Plasma Physics Reports, 2023, Vol. 49, No. 11, pp. 1251–1260. © Pleiades Publishing, Ltd., 2023.
Russian Text © The Author(s), 2023, published in Fizika Plazmy, 2023, Vol. 49, No. 11, pp. 1059–1069.

MAGNETIC TRAPS

Control of Plasma Potential in GOL-NB Axisymmetric Multiple-Mirror Trap

I. A. Ivanov[a,*], P. A. Polozova[a], V. I. Batkin[a], K. N. Kuklin[a], V. V. Kurkuchekov[a], N. A. Melnikov[a], S. V. Polosatkin[a], V. V. Postupaev[a,], A. F. Rovenskikh[a], E. N. Sidorov[a], and D. I. Skovorodin[a]**

[a] *Budker Institute of Nuclear Physics, Siberian Branch, Russian Academy of Sciences, Novosibirsk, 630090 Russia*

**e-mail: I.A.Ivanov@inp.nsk.su*

***e-mail: V.V.Postupaev@inp.nsk.su*

Received July 31, 2023; revised September 25, 2023; accepted September 25, 2023

Abstract—The results on applying the technique of vortex plasma confinement in the GOL-NB facility are presented. The first experiments on optimizing the biasing the in-chamber electrodes demonstrated an improvement in the dynamics of trapping the injected fast hydrogen atoms, as well as a decrease in the fluctuations of local plasma parameters in the central trap and an increase in the plasma decay time. The geometry of in-chamber electrodes arrangement, as well as the polarity and magnitude of the supplied potentials, correspond to the theory of vortex confinement and to those in similar studies at other open traps.

Keywords: open trap, multiple-mirror trap, GOL-NB, plasma stabilization, vortex confinement

DOI: 10.1134/S1063780X23601591

1. INTRODUCTION

Ensuring stable plasma confinement in magnetic traps is the key problem, the solution of which underlies the success of the physics research program. The most well-known method for ensuring the magnetohydrodynamic (MHD) stability is the creation of magnetic configurations that satisfy the principle of "average minimum-B" [1]. In practice, possible technical solutions are actually limited to axisymmetric systems because fast neoclassical radial diffusion occurs in the traps with multipole magnetic field components [2]. Along with the MHD-stable magnetic configurations, other methods for plasma stabilization in axisymmetric open traps are also used (see, for example, review [3]). In this article, we will consider the system of in-chamber electrodes of the GOL-NB multiple-mirror trap, designed for the forced formation of the layer with differential plasma rotation in the crossed electric and magnetic fields, and the results of optimization of its operating regimes.

Multiple-mirror magnetic systems were proposed in [4, 5] as a way to increase the plasma confinement time in open traps. In such systems, the magnetic field is corrugated (periodically modulated along the axis). When plasma expands along the magnetic field, in each elementary cell of the multiple-mirror system, the interaction of populations of transiting and locally trapped particles leads to the appearance of the friction force that slows down the plasma flow. The physics of multiple-mirror confinement and the state of work in this area are discussed in more detail in reviews [6, 7]. Currently, the multiple-mirror sections are considered as elements of the magnetic system of the GDMT new-generation open trap, which, in the full design configuration, will be able to produce plasma with sub-reactor parameters [8, 9].

The GOL-NB facility is the scaled model of the GDMT trap with the more modest technical characteristics and plasma parameters achievable [10, 11]. At this facility, the goal of research is to demonstrate the improvement of plasma parameters in the trap after activation of the multiple-mirror confinement regime and to study the basic laws of plasma flowing in the multiple-mirror magnetic field. The magnetic system of the facility does not ensure the plasma MHD stability in accordance with the criterion given in [1]. Therefore, in the physical design project of the facility [12], it was assumed that two methods would be used for the plasma MHD stabilization in the trap and reduction of transverse losses. In the stage of initial filling the trap with low-temperature starting plasma, it is quite efficient to stabilize plasma by means of the magnetic field line-tying to the well-conducting end [13, 14], which is the arc source of starting plasma. Experiments [15] generally confirmed this assumption, revealing some characteristic features in the radial dimensions of the stabilized region.

In the main stage of the GOL-NB experiment, plasma stabilization during its heating using the neu-

tral beam injection should be performed involving the differential rotation around the axis. The poloidal rotation shear is the known mechanism providing for decorrelation of turbulent transport in toroidal traps [16, 17], which ultimately results in the formation of transport barriers in tokamaks [18, 19]. In experiments at open traps, several techniques for creating the differential rotation are used: radially non-uniform heating at the electron cyclotron resonance frequency in the GAMMA 10 tandem mirror trap [20]; biasing of limiters in the Phaedrus [21] and HIEI [22] tandem mirror traps and in the GDT gasdynamic trap [23]; projection of potential from the plasma gun in the C-2 device with the field-reversed configuration (FRC) [24], and biasing of limiters and sectioned receiving endplates in the SMOLA device with a helical field [25]. Theoretical description of the physics of radial transport suppression during the differential rotation in open traps was given in [26], which used the model involving the forced formation of the radial electric field profile as plasma contacts the electrodes, and in [27], which used the closed model, in which there is no electrical contact with the ends. For the GOL-NB facility, the "vortex confinement" scheme was chosen, which is technologically simpler [23, 26]. A special reservation should be made regarding the use of the term "stabilization" in this study, as applied to the vortex confinement technique. From the formal point of view, it would be more correct to talk about the technique for limiting transverse loss using differential rotation. Differential rotation does not prevent the development of convective instabilities; it only contributes to limiting the transverse loss to some acceptable level. In further consideration, we will use the term "stabilization" with this understanding.

At the GOL-NB facility, the system for controlling the radial electric field in the plasma was developed and put into operation. It is based on biasing of different axisymmetric electrodes that are installed inside the vacuum chamber of the facility and are in contact with the plasma. The article is organized as follows. Section 2 briefly describes the GOL-NB facility. The next section describes the system of in-chamber electrodes and algorithms for supplying potentials to them. The main experimental results are presented in Section 4. The article ends with the discussion of results and summary.

2. GOL-NB FACILITY

The GOL-NB facility was designed at the Budker Institute of Nuclear Physics of the Siberian Branch of the Russian Academy of Sciences for the purpose of further development of linear magnetic confinement systems, using the technique of multiple-mirror plasma confinement [12]. It is the axisymmetric system consisting of the 2.5-m-long central trap of gasdynamic type, two adjacent high-field sections with lengths of approximately 3 m, and tanks of plasma flow expanders at the ends, see Fig. 1. Each of high-field sections consists of 28 coils and can operate in two regimes. When the coils are equally fed, the high-field section forms the solenoidal magnetic field, which acts as a long magnetic mirror. In the multiple-mirror configuration, the voltage is supplied to every second coil, and the corrugated magnetic field is formed by the thirteen elementary magnetic mirrors with corrugation period of 22 cm and corrugation depth (the mirror ratio of the multiple-mirror section) of $R_{mm} = B_{max}/B_{min} = 1.4$. The research program at the facility suggests the solution of several priority tasks (the accumulation of starting plasma in the central trap, plasma stabilization, and tests of plasma heating with neutral beams) with the solenoidal configuration of the high-field sections. Therefore, in this study, the facility operated only in the magnetic field configuration shown in the lower plot in Fig. 1. The magnetic system of expanders creates the gradually decreasing field with the expansion coefficient $K = B_{max}/B_{gun} = 36$, where the index "gun" corresponds to the coordinate of the plasma gun anode.

In the experiments described, the magnetic field configuration in the high-field sections was solenoidal with $B = 4.5$ T. In the median plane of the central trap, the field intensity was $B = 0.3$ T, so the mirror ratio was 15. In a typical experimental scenario, the central trap was at first filled with low-temperature starting plasma, which was produced by the arc plasma gun [15]. In this case, the gradual broadening of the plasma column occurs in the trap; by the end of the plasma gun operation, the density at the axis reaches $n = 4 \times 10^{19}$ m^{-3} (see [28]). According to the probe measurements in the trap, the electron temperature of the starting plasma gradually decreases from $T_e = 8$–10 eV at the beginning of the discharge to $T_e = 5$–6 eV at the end of the gun operation. Two neutral beams with the energy of $E = 25$ keV and total power of up to 1.1 MW [29] were injected into the plasma at $z = \pm 0.4$ m (the longitudinal coordinate z is measured from the median plane of the trap). A characteristic feature of the experimental scenario described was the almost simultaneous activation of the plasma gun and heating neutral beams. This was not optimal from the point of view of the efficiency of trapping fast particles by plasma, but it made possible to use neutral beams as the density diagnostics during the entire plasma discharge.

In addition to using neutral beams for measuring density, the plasma parameters were measured using the movable four-electrode Langmuir probe [30], located at $z = 0.89$ m, outside the zone of fast ions existence, which provided simultaneous measurements of the ion density, electron temperature, and radial electric field. We also used the electric probes located at $z = -0.89$ m and the magnetic probes located at $z = -0.4$ m; the spectroscopic diagnostics [31] was located at $z = 0.4$ m, and the neutral particle

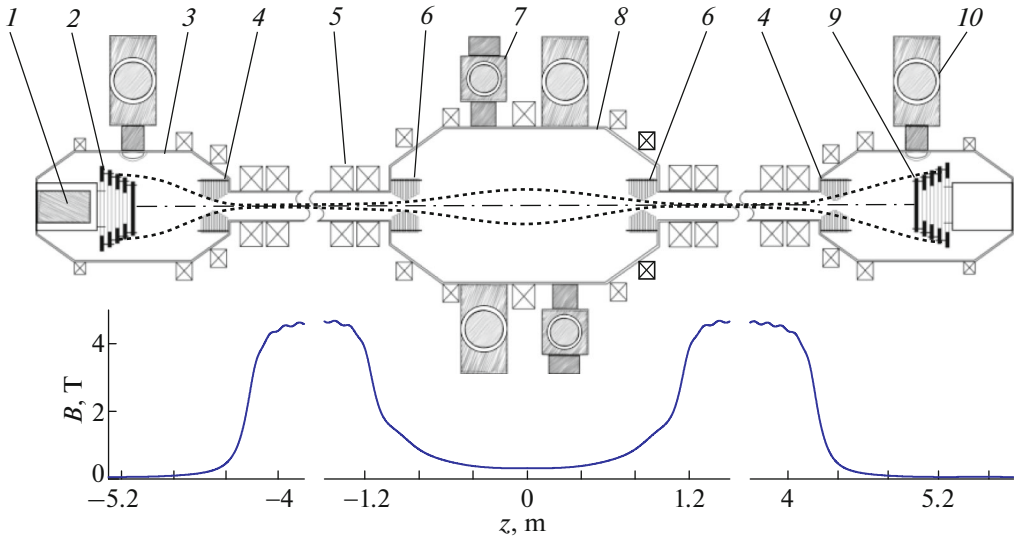

Fig. 1. Schematic of in-chamber electrodes arrangement in GOL-NB facility (top view) and magnetic induction profile along the axis: (*1*) plasma gun, (*2*) input receiving endplate sectioned in radial direction, (*3*) expander tank, (*4*) limiter assemblies inside expanders, (*5*) coil of high-field section, (*6*) limiter assemblies inside central trap, (*7*) injector of fast hydrogen atoms, (*8*) central trap, (*9*) output receiving endplate sectioned in radial direction, and (*10*) unit of pumping system. Dotted line conventionally denotes field line touching inner aperture of all limiters. The high-field sections, each consisting of 28 coils, are shown partly.

analyzer, similar to those made for the C-2 and MST [32] facilities, was located at $z = -0.4$ m.

The plasma confinement time (up to 5 ms) was limited by the duration of current pulse in the high-field coils. A more detailed description of different engineering systems of the GOL-NB device is given in [28].

3. SYSTEM FOR PLASMA POTENTIAL CONTROL

At the GOL-NB facility, the system for controlling plasma potential consists of several groups of in-chamber electrodes, which are shown in Fig. 1. During the plasma gun operation, the plasma gun cathode considerably contributes to the formation of the electric field configuration in the plasma; the cathode potential is projected into the plasma in the paraxial region. The receiving endplates (*2* and *9* in Fig. 1) are the sets of five electrodes with increasing radii. In the left receiving endplate, there is an aperture along the axis, through which the plasma flow from the gun passes. The plasma column diameter is limited by four limiter assemblies (*4* and *6* in Fig. 1), located in the decreasing magnetic field near the magnetic mirrors outside the region, in which the fast ions population exists. All in-chamber electrodes are made of molybdenum in order to reduce the probability of unipolar arcing. High-density Al_2O_3 ceramics is used for insulators.

The shape and location of the plasma receiving endplates installed in the magnetic field expanders, which receive the plasma escaping the trap, as well as the plasma gun geometry, are described in detail in [15, 33]. The characteristic features of the plasma receiving endplates are their radial sectioning; the plates are electrically insulated disks with gradually increasing diameters and individual biasing. The limiter assemblies are installed at both sides of the high-field sections. They are sets of ten 0.5-mm-thick rings with the diameters of inner apertures gradually increasing from the assembly center to its edges. The two middle rings are electrically connected. They can be either biased from the external power source or these electrodes can be left under the floating potential. The rest of electrodes of the limiter assemblies are protective. During the facility operation, they acquire the floating potential. The limiter assemblies are located in ≈1 T magnetic field. Due to the pulsed powering of the high-field coils with a current rise time of approximately 13 ms, the ring electrodes of the limiter assemblies have radial cuts to eliminate the possibility of their destruction as a result of the eddy currents excitation.

The electrical connection scheme of the in-chamber electrodes is a compromise between the problems of ensuring plasma stability and forming the maximum flow of starting plasma particles from the plasma gun into the central trap. Table 1 shows some geometrical parameters of the in-chamber electrodes: the longitudinal coordinate, local magnetic field B, local mirror ratio $R = B_{max}/B$, and diameter of the field tube projection onto the center of the trap with $z = 0$. As can be seen, all limiter assemblies are installed almost on the same magnetic surface (with a small deviation), and the magnetic fluxes are matched with an accuracy

Table 1. Basic parameters of intrachamber electrodes of GOL-NB

Designation	z, m	B, T	D, mm	R	$D_{z=0}$, mm
Aperture in plasma gun anode	−5.29	0.122	45	36	29
Aperture in central receiving endplate	−5.11	0.082	180	55	95
Middle ring of left receiving endplate	−5.14	0.089	500	50	276
Limiters of expanders	±4.31	0.96	145	4.7	263
Limiters of central trap	±1.02	1.71	110	2.6	266
Middle ring of right receiving endplate	5.14	0.062	560	73	260

of better than 2%. Due to different current rise times in different coils of the magnetic system and the occurrence of considerable eddy currents in the vacuum chamber, perfect matching throughout the entire duration of the experiment is not possible.

In order to avoid direct electrical connection along the magnetic field with the receiving endplates, the inner limiters (located in the central trap) are installed in the shadow of the outer ones (located in the expanders). This was done because the vortex confinement technique adopted for the GOL-NB device [23, 26] involves the supply of potentials of opposite polarity to the receiving endplates and limiters of the central section. Therefore, the limiters installed in the expanders, being under the floating potential, block the direct current between the receiving endplates and inner limiters. In turn, only the radial component of the current flowing from the limiters in the central cell to the receiving endplates makes the plasma rotate due to the Ampere force. The radial step $\Delta r = 2$ mm between the electrodes of the limiter assemblies was chosen several times larger than the ion Larmor radius of the plasma thermal component, which can reach a temperature of several tens of electronvolts in later experiments.

Currently, at the GOL-NB facility, the biasing circuit for in-chamber electrodes is as follows. The receiving endplates of the left expander are grounded through the resistive divider with the uniform step $R = 0.32\ \Omega$. This measure reduces the possibility of switching the high-current discharge in the plasma gun onto the vacuum chamber body and increases the efficiency of producing plasma and transporting it along the long solenoid. The electrodes potentials of the receiving endplate increase from the edge to the axis. Currently, the connection of the left receiving endplates is passive; the plates potentials are determined by plasma processes. If necessary, the GOL-NB design allows to change the distribution of their potentials using external power supply sources. The right receiving endplates can be negatively biased with independent supplies in the range of 0–250 V. Usually, these voltages were set so that their amplitudes increase in equal increments towards the central disk. The positive potentials in the range of 0–200 V were supplied synchronously to the middle electrodes of the inner limiters before starting the plasma generator and they remain constant during the discharge. Typical waveforms of currents of all active in-chamber electrodes are shown in Fig. 2. As can be seen, the current amplitudes do not exceed 100 A. They are comparable in current densities with the currents of ion or electron saturation of the Langmuir probes (in accordance with the polarity of the applied potentials).

The in-chamber electrodes power supply system uses the 1.5 kW AC-DC controlled sources with galvanically isolated outputs, which provide the output voltage in the range of 15–55 V. Series connection of five such sources enables biasing from ±15 to ±275 V to the central electrode of the receiving endplate of the facility. In order to increase the pulsed current, the outputs of all sources are connected to 6.8-mF capacitors. Commutation to the load is performed using the IGBT switches that have sufficient load margin. To control the source output voltage and timing of switching on the transistors, the special circuit was created based on the circuit board with the 32-bit STM32F407 microcontroller of the Cortex M4 architecture. First, it controls the output voltages of the AC-DC sources using the galvanically insulated channels of digital-to-analog converters. The microcon-

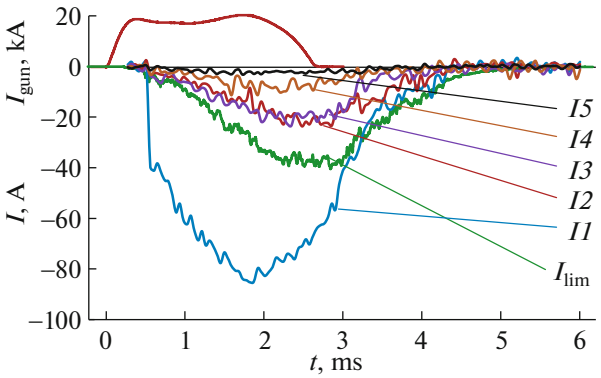

Fig. 2. Typical signals characterizing operation of power supply systems of intracameral electrodes. Plasma gun current is given to illustrate time scale; radial segments of receiving endplate are numbered from center to edge as *I1–I5*. For clarity, currents of plasma gun I_{gun} and limiters I_{lim} are shown with reverse polarity.

troller also controls the AC-DC sources switching on/off and monitors their states. The measurements of analog signals of the output voltage and current are provided by the same circuit board. This creates the self-consistent system with reduced interference in the measuring channels. Communication with the GOL-NB control and data acquisition system uses the Ethernet 1000base-T network.

4. EFFECT OF POTENTIALS ON PLASMA PARAMETERS

The positive effect of applying the negative potential to the receiving endplates on the efficiency of plasma transport along the high-field section was previously shown in experiments performed in the starting GOL-NB configuration [33]. Therefore, the main goal of the experiments presented was to determine the optimal operating regime of the entire system of in-chamber electrodes, mainly the limiters. Figure 3 shows typical signals obtained at different limiter potentials. In all cases, the potential of the right receiving endplate was equal to $U_r = -200$ V. Here and hereinafter, for denoting the operating regime of the device, we will use the voltage set by the power source. The real potential supplied into the plasma changes during the discharge due to some potential drop at the protective resistor, which limits the breakdown current, as well as due to the changes in the potential drop occurring in the Langmuir layer due to the time evolution of the surface plasma parameters. At the top in Fig. 3, the discharge current of the plasma gun and the total current onto the limiters of the central section are shown. The figure shows time evolution of the current onto the right output receiving endplate, as well as the currents of transiting fast atoms, recorded along the central chord. It can be seen that as the positive potential of the limiters increases, the trapping of heating beams becomes better. This indicates a better accumulation of the starting plasma density in the trap with a positive biasing of the limiters. For potentials $U_{lim} = +100$ and $+200$ V, the currents to the limiters considerably differ, but this does not result in additional enhancement of the beam trapping, despite the increase in the current to the limiters. We note that the electric power $U_{lim}I_{lim} \approx 5-10$ kW supplied to the limiters is rather small to considerably affect the plasma parameters in the trap.

The signals in Fig. 3e show the escape dynamics of fast atoms born due to charge exchange of trapped fast protons (25 keV channel of the neutral particle analyzer). This parameter is proportional to three plasma parameters at the point of beam injection:

$$P \propto I_b n_g \int n dr,$$

where I_b is the equivalent current of the injected beam, n_g is the gas density in the region of fast protons confinement, and the integration is performed along the observation chord. The figure demonstrates the following. In the regime with grounded limiters, the higher density of neutral gas is observed as compared to the regime, in which the positive potential is applied to the limiter. In addition, with the grounded limiter, after switching off the plasma gun, the plasma decays faster than in the case of the negative potential applied to the limiters.

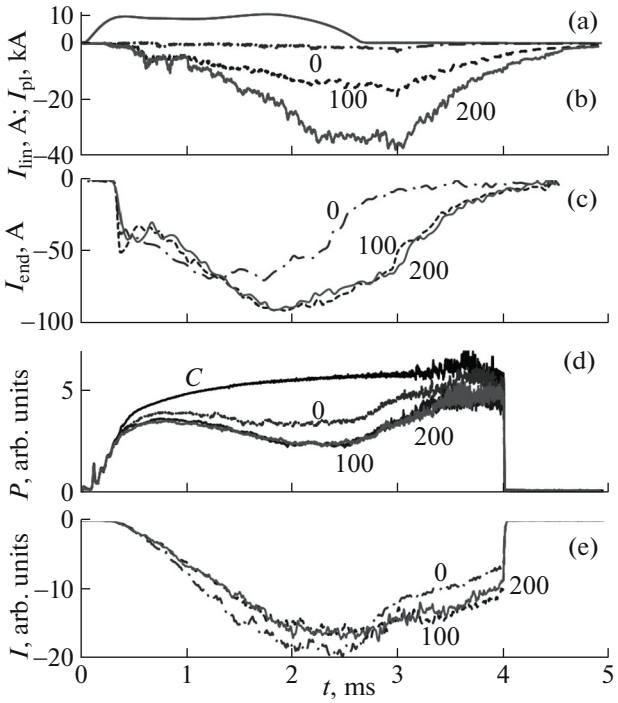

Fig. 3. Signals at different limiter potentials in central trap (labels at the curves correspond to potentials in volts): (a) discharge current in plasma gun; (b) total current of two limiters in central trap; (c) current in central section of output receiving endplate; (d) current density of heating neutral beam that passed through vacuum chamber (C is signal measured in control experiment without plasma; the lower is signal with plasma, the better is beam trapping coefficient); and (e) flux of charge-exchange neutrals in channel with energy of 25 keV.

The radial potential distribution in the plasma of the central trap was measured using the routine 4-mm-long cylindrical electric probe. The probe could be displaced along the radius within the 102-mm-long segment. The floating potential of the probe was measured, which, as is known, differs from the plasma potential by the potential drop in the Langmuir layer. Figure 4 shows radial potential profiles measured at the limiter potential $U_{lim} = 100$ V at two typical times: in the stage of plasma accumulation (2 ms) and in the decay stage (3 ms). It can be seen that near the limiter, the layer with varying electric field is actually formed, in which the plasma differential rotation should occur due to the $\mathbf{E} \times \mathbf{B}$ drift. Currently, the velocity of the plasma rotation is not

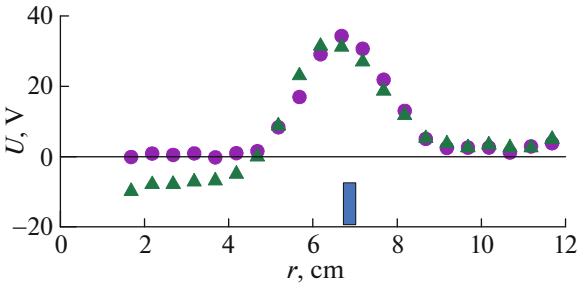

Fig. 4. Potential of electrostatic probe, installed at z = 0.89 m, relative to facility body at two times: t = 2 ms (circles) and t = 3 ms (triangles). Rectangle at coordinates 6.7–7 cm symbolically shows projection of radial position of limiter ring, to which potential is supplied.

directly measured at this point, but it can be estimated from the measured radial electric field. In this operating regime of the facility, $E_r \approx 20$ V/cm at $r \approx 5.5$ cm; therefore, at this radius, the velocity of $\mathbf{E} \times \mathbf{B}$ drift is $v_\varphi \approx 1.7 \times 10^5$ cm/s and the angular velocity of plasma rotation is $\omega \approx 3 \times 10^4$ s^{-1}. With increasing distance from the region of maximum potential gradient, the electric field and the velocity of drift rotation decrease; in the region beyond the limiter, the plasma rotates in the opposite direction.

In the region beyond the limiter, the potential is self-consistently formed as a result of contact of the low-density limiter plasma with the radially sectioned protective electrodes of the limiter assembly, which acquire the floating potential. In the central part of the plasma column, in the stages of plasma accumulation and decay, the dynamics of potential are different. As can be seen in Fig. 4, in the central trap, during the plasma gun operation, the potential of the paraxial region is close to zero. It is determined by good electrical contact of the plasma with the emitting dense anode plasma of the high-current discharge in the plasma gun. After the discharge in the plasma gun terminates and the conduction near this endplate of the facility degrades, the plasma potential in the trap begins to be determined by the translation of the potential from the output receiving endplate side. In this case, the central plasma region acquires the negative potential, and the zone of differential rotation expands. We note that in this regime, the voltage drop across the protective resistors installed in the feed circuit is within 5–10 V. The potential drop in the Langmuir layer at the electrodes and at the probe can be estimated as $\Delta\varphi \approx 3.3 T_e/e \approx 20$ V. Thus, we could state the reasonable agreement between the measured potential at the maximum of the curves in Fig. 4 with the voltage set by the power source.

Considering in detail the behavior of currents flowing onto the limiters and receiving endplates, we can quantitatively characterize the plasma confinement time in the trap after the plasma gun is switched off.

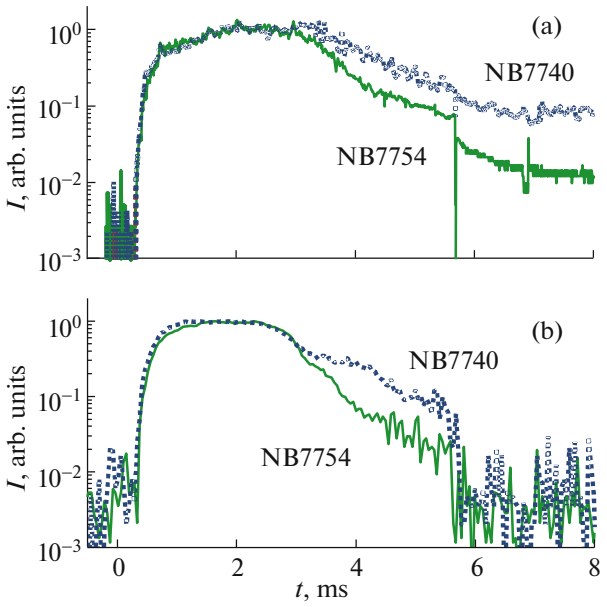

Fig. 5. Total currents onto (a) limiters and (b) right central receiving endplate, normalized to their maximum amplitudes, at different supplied potentials: in experiment NB7754, $U_{\rm lim}$ = +50 V, U_r = –250 V, and in experiment NB7740, $U_{\rm lim}$ = +100 V, U_r = –120 V. Signal jumps at t = 5.7 ms correspond to switching off supply of potentials to receiving endplate.

During this time interval, the plasma density rapidly decreases and the density diagnostics by the attenuation of neutral beams becomes highly inaccurate. The in-chamber electrodes can be considered as the macroscopic Langmuir probes. Therefore, within the corresponding magnetic surfaces, the ion current is collected by the receiving endplates, and the electron current is collected by the limiters. In this regard, to reduce the effect of the current-voltage characteristics, in Fig. 5, the signals of these currents are shown normalized to their maxima in each presented experiment. As can be seen in Fig. 5a, after switching off the plasma gun discharge at t_0 = 2.7 ms, the current flowing to the limiters decreases exponentially. In this case, in the time interval t = 2.7–4 ms, the exponent considerably depends on the potentials of the receiving endplate and limiters. Such behavior of the current flowing onto the limiters can be interpreted as an increase in the plasma confinement time in the central trap.

The fall time of the current to the limiters as a function of the receiving endplate potential is shown in Fig. 6a. In the regime under consideration, the potential of the limiters was within the range of $U_{\rm lim}$ = 100–150 V. The shown error bars correspond to the dispersion of the parameters measured in a series of shots. As can be seen, under optimal biasing conditions, this time is already comparable in order of magnitude with the estimate of the gas-dynamic confinement time: $\tau \sim RL/2c_s \sim 0.5$ ms, where R = 15 is the mirror ratio,

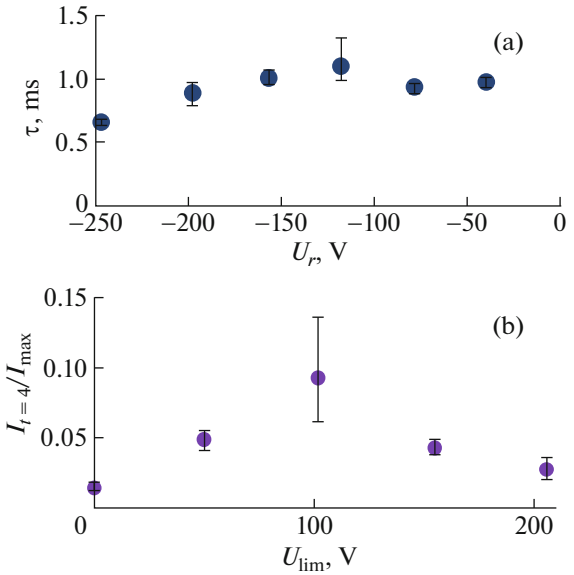

Fig. 6. (a) Time of exponential decay of current onto limiters after switching off plasma gun as a function of voltage amplitude at receiving endplate; and (b) ratio between current onto receiving endplate at $t = 4$ ms to maximal current as a function of voltage at limiter. Error bars correspond to dispersion of measured parameters in a series of experiments.

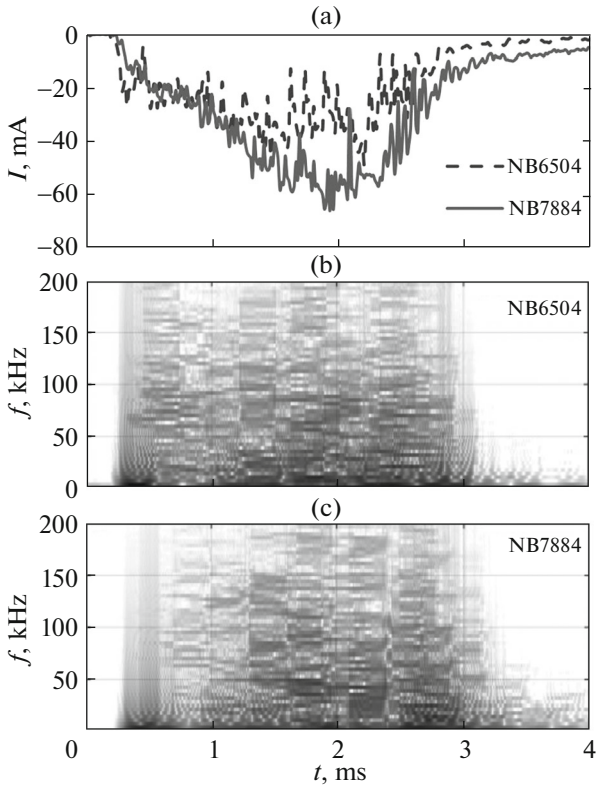

Fig. 7. (a) Signals of double Langmuir probe installed in central trap at $z = 0.89$ m in experiments without neutral beam injection at two limiter potentials: (NB6504) 0 and (NB7884) +100 V; (b) and (c) spectrograms of Langmuir probe current signals in experiments NB6504 and NB7884, respectively. Color intensity corresponds to harmonic amplitude in logarithmic scale.

L is the trap length, and c_s is the sound velocity. Figure 6b shows the ratio of the current to the receiving endplate at $t = 4$ ms to its maximum. The higher is this ratio, the more efficiently is the plasma confined in the trap after the discharge current in the plasma gun is switched off and the stabilizing effect of line-tying into the gun plasma disappears.

As a result of this series of experiments, the optimal potentials of the limiters ($U_{lim} = 100$ V) and receiving endplates ($U_r = -120$ V) were found. Further we will compare other experiments on identifying the effect of biasing on the behavior of local plasma parameters with this optimal operating regime.

First, we performed a series of experiments on measuring the local plasma density fluctuations in the cross-section of the central trap in the region between the stopping point of fast protons and the limiters. The movable double Langmuir probe was installed in this cross-section and displaced along the radius in pauses between experiments. The ion saturation currents of the probe located at the plasma axis at different limiter potentials are shown in Fig. 7a. In these experiments, the potential of the receiving endplates was $U_r = -150$ V. As can be seen from the signals presented, the positive bias of the limiters results in an increase in the plasma density and confinement time. The signals of the probe saturation current are rather noisy, and the noise amplitude depends on the supplied potential. The Fourier spectrograms with the running window of 0.25 ms are shown in Figs. 7b and 7c. Two facts are clear from these spectrograms. Firstly, when the limiters are posivitely biased, a decrease in the amplitudes of high-frequency modes is observed. Secondly, when the plasma gun discharge current is switched off, in the time interval $t \approx 2.5$–3 ms, the quasi-harmonic oscillations at the frequency of $f \approx 13$ kHz and at its harmonics appear in the signals. For the grounded limiters $U_{lim} = 0$, these oscillations periodically occur even during the discharge of the plasma gun. After the gun is switched off, they occur somewhat earlier than in the case of the positive biasing of the limiters. This indirectly indicates a stronger MHD activity, which results in the rapid loss of particles across the magnetic field at zero bias.

Further the plasma behavior studies behind the limiters were done with the electrostatic probe. It records the difference in floating potentials between two electrodes displaced in the azimuthal direction by 1 cm. The measuring head of the probe was located deep in the shadow of the limiters at $z = -0.89$ m and $r = 115$ mm, which corresponds to the distance $\Delta r = 100$ mm to the last closed magnetic surface set by the limiters (as recalculated to the magnetic field strength

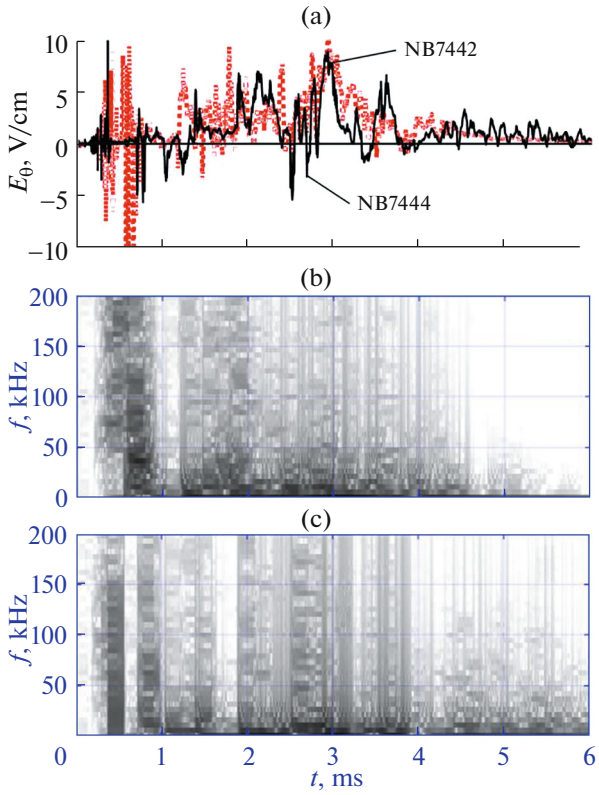

Fig. 8. (a) Azimuthal electric field strength E_θ in shadow of limiter (projection of radius onto central plane $R = 23$ cm) at different potentials $U_{lim} = 0$ (NB7442) and $U_{lim} = 100$ V (NB7444); (b) and (c) mode composition of azimuthal electric field oscillations according to signals in Fig. 8a in experiments NB7442 and NB7444, respectively. The darker is spectral line, the higher is amplitude of harmonic in logarithmic scale.

in the median plane of the central trap). From the mechanical point of view, the probe electrodes are the thoriated tungsten wires with a diameter of 0.1 mm and a length of 4 mm. When measuring the potential difference, the signal was fed to the differential amplifier with the analog bandwidth of $f < 13$ MHz, which suppressed common-mode noise. The probe signals, converted to the azimuthal electric field, are shown in Fig. 8 for two cases: the optimal regime of supplying potentials to in-chamber electrodes (experiment NB7444) and the regime with grounded limiters (experiment NB7442). The mode composition of the azimuthal field oscillations is also shown there. Spectrograms were calculated using the fast Fourier transform with the sliding window of 0.25 ms. The main conclusion derived from the above spectrograms is that in plasma escaping across the magnetic field, the amplitude of fluctuations is considerable only in the low-frequency range. The same as in the diagrams of the Langmuir probe signal shown in Fig. 7, the fluctuations occur in the frequency band including $f =$ 10 kHz and its nearest harmonics. In addition, we note that in the case of the optimal biasing of the limiters, the azimuthal electric field amplitude is somewhat lower, the oscillation spectrum is narrower, and the signal duration is longer. This indicates the lower intensity of the MHD plasma activity in the peripheral region. For the above shots, in the case of the optimal biasing, the mean amplitude of the azimuthal electric field strength is ~30% lower than that in the regime with grounded limiters. This is qualitatively consistent with the increase in beam trapping shown in Fig. 3.

5. DISCUSSION AND SUMMARY

At the GOL-NB facility, the system for creating the radial electric field in plasma was designed, tested and put into operation. This radial electric field is required for the formation of the plasma layer with differential rotation around the axis due to the drift in crossed electric and magnetic fields. This is necessary for limiting the amplitude of interchange instabilities using the vortex confinement technique [23, 26]; otherwise, these instabilities result in the high transverse plasma loss. The system consists of five-electrode receiving endplates sectioned in radial direction, two limiter assemblies in the central trap, two limiter assemblies in the expander tanks, controlled power supply sources, and instruments for measuring currents and applied potentials. The first experiments on optimizing the biasing of these systems were performed. An improvement in the dynamics of trapping the injected fast hydrogen atoms was experimentally demonstrated, as well as a decrease in fluctuations of the local plasma parameters in the central section of the trap, after the optimal voltages were supplied to the intrachamber electrodes. It is important that the most significant improvements in plasma parameters were observed after the plasma gun switches off, when the stabilization due to line-tying of the magnetic field into the conducting end plasma of the high-current discharge in the gun disappears.

In the experiments presented, the geometry of the electrodes, polarities and potentials correspond to those expected based on the theory of vortex confinement and experiments at the GDT facility [26], on which the authors relied when designing the GOL-NB facility. The optimum in terms of the electrode potentials is rather smooth (see Fig. 5); however, after stabilization due to line-tying ceases, the improvement in the plasma confinement time in the trap is considerable. If the voltage becomes higher than the optimal one, the degradation of confinement due to the increasing destabilization caused by the Kelvin–Helmholtz instability is observed, as is predicted in theory [23, 26]. We note that in the theory of vortex confinement, the population of fast ions formed due to trapping neutral particles from heating beams considerably contributes to stabilization. In the first experiments with neutral beam injection at GOL-NB [34], the loss of fast ions due to charge exchange was

observed, because of which the fast ion density and plasma temperature were lower than those calculated. As the plasma temperature and fast ion density increase, the potentials optimal in terms of confinement should increase, so the existing voltage reserves of the power supply systems can be used.

In conclusion, we note one more circumstance. Any real experiment is a rather complex event, in the course of which different processes occur simultaneously. A change in one of the experimental parameters often leads to simultaneous changes in several processes, and it is difficult or even impossible to isolate the contribution of each of them to the changes in the final result. One of these processes is the longitudinal current flowing through the plasma. The amplitude of this current depends on the voltages supplied (see Fig. 3). In the above consideration, we already mentioned the Ohmic heating power released by the flowing current and somewhat modifying the plasma parameters. Another effect of the flowing current is the appearance of the global azimuthal magnetic field. As is well known, in linear systems, the limiting longitudinal current (in terms of the criterion of [35, 36]) is determined by the following expression (in SI units):

$$q = \frac{2\pi a}{L}\frac{B_z}{B_\theta} = \frac{(2\pi a)^2 B_z}{\mu_0 L I} > 1,$$

where q is the stability factor, μ_0 and B_θ are the axial and azimuthal components of the magnetic field, respectively, a and L are the plasma radius and length, respectively, μ_0 is the permeability of free space, and I is the total plasma current. For the parameters of the GOL-NB facility, the maximum acceptable longitudinal current exceeds 15 kA, which is many times more than the plasma current in this experiment. In this work, we studied operation of the system of in-chamber electrodes at their symmetrical connection. The asymmetrical connection is also possible, which means that different potentials will be supplied to the limiters, and the longitudinal current will additionally occur between them. Then, in addition to the rotation shear, the magnetic field shear will also exist, which is also a stabilizing factor [37]. Since the potentials of limiters and receiving endplates are set independently and have different polarities, in principle, it is possible that the current directions near the plasma axis and at the edge will be opposite. Previously, in experiments at the GOL-3 facility, it was shown [38] that such a configuration can provide for the MHD stabilization of the configuration that is unstable in terms of the criterion given in [1], even for $q < 1$ at the system axis. The current flowing at the edge of the system with low density will also serve as an additional source of the Ohmic heating in that region. Similar regime of high-current operation of ring electrodes is used in experiments at the C-2W device [39].

When this article was under reviewing, the paper on the physical basis of the WHAM facility was published [40], which described the electrode system for similar plasma stabilization technique with the formation of the differential rotation layer.

FUNDING

The construction and operation of the GOL-NB facility was supported by the Ministry of Science and Higher Education of the Russian Federation. The studies of plasma stability were supported by the Russian Science Foundation (project no. 21-12-00133). https://rscf.ru/en/project/21-12-00133/.

CONFLICT OF INTEREST

The authors of this work declare that they have no conflicts of interest.

REFERENCES

1. M. N. Rosenbluth and C. L. Longmire, Ann. Phys. **1**, 120 (1957). https://doi.org/10.1016/0003-4916(57)90055-6
2. D. D. Ryutov and G. V. Stupakov, JETP Lett. **26**, 174 (1977).
3. D. D. Ryutov, H. L. Berk, B. I. Cohen, A. W. Molvik, and T. C. Simonen, Phys. Plasmas **18**, 092301 (2011). https://doi.org/10.1063/1.3624763
4. G. I. Budker, V. V. Mirnov, and D. D. Ryutov, JETP Lett. **14**, 212 (1971).
5. B. Grant Logan, A. J. Lichtenberg, M. A. Lieberman, and A. Makhijani, Phys. Rev. Lett. **28**, 144 (1972). https://doi.org/10.1103/PhysRevLett.28.144
6. A. J. Lichtenberg and V. V. Mirnov, in *Reviews of Plasma Physics*, Ed. by B. B. Kadomtsev (Consultants Bureau, New York, 1996), Vol. 19, p. 53.
7. A. V. Burdakov and V. V. Postupaev, Phys.—Usp. **61**, 582 (2018). https://doi.org/10.3367/UFNe.2018.03.038342
8. P. A. Bagryansky, A. D. Beklemishev, and V. V. Postupaev, J. Fusion Energy **38**, 162 (2019). https://doi.org/10.1007/s10894-018-0174-1
9. D. I. Skovorodin, I. S. Chernoshtanov, V. Kh. Amirov, V. T. Astrelin, P. A. Bagryanskii, A. D. Beklemishev, A. V. Burdakov, A. I. Gorbovskii, I. A. Kotel'nikov, E. M. Magommedov, S. V. Polosatkin, V. V. Postupaev, V. V. Prikhod'ko, V. Ya. Savkin, E. I. Soldatkina, et al., Plasma Phys. Rep. **49**, 1039 (2023). https://doi.org/10.1134/S1063780X23600986
10. V. V. Postupaev, A. V. Burdakov, and A. A. Ivanov, Fusion Sci. Technol. **68**, 92 (2015). https://doi.org/10.13182/FST14-846
11. V. V. Postupaev and D. V. Yurov, Plasma Phys. Rep. **42**, 1013 (2016). https://doi.org/10.1134/S1063780X16110076
12. V. V. Postupaev, V. I. Batkin, A. D. Beklemishev, A. V. Burdakov, V. S. Burmasov, I. S. Chernoshtanov, A. I. Gorbovsky, I. A. Ivanov, K. N. Kuklin, K. I. Mekler, A. F. Rovenskikh, E. N. Sidorov, and D. V. Yurov, Nucl. Fusion **57**, 036012 (2017). https://doi.org/10.1088/1741-4326/57/3/036012

13. R. Prater, Phys. Fluids **17**, 193 (1974). https://doi.org/10.1063/1.1694587
14. A. W. Molvik, R. A. Breun, S. N. Golovato, N. Hershkowitz, B. McVey, R. S. Post, D. Smatlak, and L. Yujiri, Phys. Fluids **27**, 2711 (1984). https://doi.org/10.1063/1.864575
15. I. A. Ivanov, V. I. Batkin, A. V. Burdakov, K. N. Kuklin, K. I. Mekler, V. V. Postupaev, A. F. Rovenskikh, and E. N. Sidorov, Plasma Phys. Rep. **47**, 938 (2021). https://doi.org/10.1134/S1063780X21090026
16. K. C. Shaing and E. C. Crume, Jr., Phys. Rev. Lett. **63**, 2369 (1989). https://doi.org/10.1103/PhysRevLett.63.2369
17. H. Biglari, P. H. Diamond, and P. W. Terry, Phys. Fluids B **2**, 1 (1990). https://doi.org/10.1063/1.859529
18. T. S. Taylor, Plasma Phys. Controlled Fusion **39**, B47 (1997). https://doi.org/10.1088/0741-3335/39/12B/005
19. K. H. Burrell, Phys. Plasmas **4**, 1499 (1997). https://doi.org/10.1063/1.872367
20. T. Cho, M. Yoshida, J. Kohagura, M. Hirata, T. Numakura, H. Higaki, H. Hojo, M. Ichimura, K. Ishii, K. Md. Islam, A. Itakura, I. Katanuma, Y. Nakashima, T. Saito, Y. Tatematsu, et al., Phys. Rev. Lett. **94**, 085002 (2005). https://doi.org/10.1103/PhysRevLett.94.085002
21. G. D. Severn, N. Hershkowitz, R. A. Breun, and J. R. Ferron, Phys. Fluids B **3**, 114 (1991). https://doi.org/10.1063/1.859948
22. O. Sakai, Y. Yasaka, and R. Itatani, Phys. Rev. Lett. **70**, 4071 (1993). https://doi.org/10.1103/PhysRevLett.70.4071
23. A. D. Beklemishev, P. A. Bagryansky, M. S. Chaschin, and E. I. Soldatkina, Fusion Sci. Technol. **57**, 351 (2010). https://doi.org/10.13182/FST10-A9497
24. L. Schmitz, D. Fulton, E. Ruskov, C. Lau, B. H. Deng, T. Tajima, M. W. Binderbauer, I. Holod, Z. Lin, H. Gota, M. Tuszewski, S. A. Dettrick, and L. C. Steinhauer, Nat. Commun. **7**, 13860 (2016). https://doi.org/10.1038/ncomms13860
25. A. V. Sudnikov, A. D. Beklemishev, V. V. Postupaev, A. V. Burdakov, I. A. Ivanov, N. G. Vasilyeva, K. N. Kuklin, and E. N. Sidorov, Fusion Eng. Des. **122**, 86 (2017). https://doi.org/10.1016/j.fusengdes.2017.09.005
26. A. D. Beklemishev, AIP Conf. Proc. **1069**, 3 (2008). https://doi.org/10.1063/1.3033729
27. V. P. Pastukhov and V. N. Chudin, Fusion Sci. Technol. **59**, 84 (2011). https://doi.org/10.13182/FST11-A11580
28. V. V. Postupaev, V. I. Batkin, A. V. Burdakov, V. S. Burmasov, I. A. Ivanov, K. N. Kuklin, Yu. A. Lykova, N. A. Melnikov, K. I. Mekler, A. V. Nikishin, S. V. Polosatkin, A. F. Rovenskikh, E. N. Sidorov, and D. I. Skovorodin, Nucl. Fusion **62**, 086003 (2022). https://doi.org/10.1088/1741-4326/ac69fa
29. V. I. Batkin, E. E. Bambutsa, A. V. Burdakov, V. S. Burmasov, M. R. Gafarov, and R. V. Voskoboinikov, AIP Conf. Proc. **1771**, 030010 (2016). https://doi.org/10.1063/1.4964166
30. E. N. Sidorov, V. I. Batkin, A. V. Burdakov, I. A. Ivanov, K. N. Kuklin, K. I. Mekler, A. V. Nikishin, V. V. Postupaev, and A. F. Rovenskikh, J. Instrum. **16**, T11006 (2021). https://doi.org/10.1088/1748-0221/16/11/T11006
31. A. V. Nikishin, I. A. Ivanov, V. I. Batkin, A. V. Burdakov, K. N. Kuklin, K. I. Mekler, V. V. Postupaev, and A. F. Rovenskikh, Plasma Phys. Rep. **48**, 220 (2022). https://doi.org/10.1134/S1063780X22030114
32. S. Polosatkin, V. Belykh, V. Davydenko, R. Clary, G. Fiksel, A. Ivanov, V. Kapitonov, D. Liu, V. Mishagin, M. Tiunov, and R. Voskoboynikov, Nucl. Instrum. Methods Phys. Res., Sect. A **720**, 42 (2013). https://doi.org/10.1016/j.nima.2012.12.039
33. V. V. Postupaev, V. I. Batkin, A. V. Burdakov, V. S. Burmasov, I. A. Ivanov, K. N. Kuklin, K. I. Mekler, A. F. Rovenskikh, and E. N. Sidorov, Plasma Phys. Controlled Fusion **62**, 025008 (2020). https://doi.org/10.1088/1361-6587/ab53c2
34. V. V. Postupaev, V. I. Batkin, A. V. Burdakov, V. S. Burmasov, I. A. Ivanov, K. N. Kuklin, Yu. A. Lykova, K. I. Mekler, N. A. Mel'nikov, A. V. Nikishin, S. V. Polosatkin, A. F. Rovenskikh, E. N. Sidorov, V. F. Sklyarov, and D. I. Skovorodin, Plasma Phys. Rep. **48**, 1137 (2022). https://doi.org/10.1134/S1063780X22600682
35. V. D. Shafranov, Sov. J. At. Energy **1**, 709 (1956). https://doi.org/10.1007/BF01480907
36. M. D. Kruskal, J. L. Johnson, M. B. Gottlieb, and L. M. Goldman, Phys. Fluids **1**, 421 (1958). https://doi.org/10.1063/1.1724359
37. B. R. Suydam, in *Proceedings of the 2nd United Nations International Conference on Peaceful Uses of Atomic Energy, Geneva, 1958*, Vol. 31, p. 354.
38. A. V. Burdakov, V. V. Postupaev, and A. V. Sudnikov, Phys. Plasmas **21**, 052507 (2014). https://doi.org/10.1063/1.4876745
39. H. Gota, M. W. Binderbauer, T. Tajima, S. Putvinski, M. Tuszewski, B. H. Deng, S. A. Dettrick, D. K. Gupta, S. Korepanov, R. M. Magee, T. Roche, J. A. Romero, A. Smirnov, V. Sokolov, Y. Song, et al., Nucl. Fusion **59**, 112009 (2019). https://doi.org/10.1088/1741-4326/ab0be9
40. D. Endrizzi, J. K. Anderson, M. Brown, J. Egedal, B. Geiger, R. W. Harvey, M. Ialovega, J. Kirch, E. Peterson, Yu. V. Petrov, J. Pizzo, T. Qian, K. Sanwalka, O. Schmitz, J. Wallace, et al., J. Plasma Phys. **89**, 975890501 (2023). https://doi.org/10.1017/S0022377823000806

Translated by I. Grishina

Publisher's Note. Pleiades Publishing remains neutral with regard to jurisdictional claims in published maps and institutional affiliations.